

Spherical Accretion to a Magnetized Neutron Star in the "Propeller" Regime

O.D. Toropina¹, M.M. Romanova², Yu.M. Toropin³, and R.V.E. Lovelace²

¹ Space Research Institute, Moscow, Russia, e-mail: toropina@iki.rssi.ru

² Department of Astronomy, Cornell University, USA

³ CQG International Ltd, Moscow, Russia

Abstract. We investigate spherical accretion to a rotating magnetized star in the "propeller" regime using axisymmetric resistive magnetohydrodynamic simulations. In this regime accreting matter tends to be expelled from the equatorial region of the magnetosphere where the centrifugal force on matter rotating with the star exceeds the gravitational force. The regime is predicted to occur if the magnetospheric radius is larger than the corotation radius and smaller than the light cylinder radius. The simulations show that accreting matter is expelled from the equatorial region of the magnetosphere and that it moves away from the star in a supersonic, disk-shaped outflow. At larger radial distances the outflow slows down and becomes subsonic. The equatorial matter outflow is initially driven by the centrifugal force, but at larger distances the pressure gradient force becomes significant. We find that the fraction of the Bondi accretion rate which accretes to the surface of the star is found to be $\propto \Omega_*^{-1.0} \mu^{-2.1} \eta_m^{0.7}$. Predictions of this work are important for the observability of isolated old neutron stars and for wind fed pulsars in X-ray binaries.

Key words. MHD, neutron stars, accretion, magnetic field, propeller regime.

1. Introduction

Rotating magnetized neutron stars pass through different stages in their evolution (Shapiro & Teukolsky 1983), (Lipunov 1992). Initially, a rapidly rotating ($P \leq 1$ s) magnetized neutron star is expected to be active as a radiopulsar. The star spins down owing to the wind of magnetic field and relativistic particles from the region of the light cylinder r_L (Goldreich & Julian 1969). However, after the neutron star spins-down sufficiently, the light cylinder radius becomes larger than magnetospheric radius r_m where

the ram pressure of external matter equals the magnetic pressure in the neutron star's dipole field. The relativistic wind is then suppressed by the inflowing matter (Shvartsman 1970). The external matter may come from the wind from a binary companion or from the interstellar medium for an isolated neutron star. The centrifugal force in the equatorial region at r_m is much larger than gravitational force if r_m is much larger than the corotation radius r_{cor} . In this case the incoming matter tends to be flung away from the neutron star by its rotating magnetic field. This is the so called "propeller" stage of evolution (Davidson & Ostriker, J.P. 1973), (Illarionov & Sunyaev 1975).

Send offprint requests to: O.D. Toropina

The "propeller" stage of evolution, though important, is still not well-understood theoretically. We discuss results of axisymmetric, two-dimensional, resistive MHD simulations of accretion to a rotating magnetized star in the "propeller" regime. We treat the case when matter accretes spherically with the Bondi accretion rate (Bondi 1952). Bondi accretion to a non-rotating and a slowly rotating star was investigated by Toropin et al. (Toropin et al. 1999) and Toropina et al. (Toropina et al. 2003). Investigation of the accretion to a rotating star in the "propeller" regime was started by Romanova et al. (Romanova et al. 2003).

2. Model

We simulate the plasma flow in the propeller regime using an axisymmetric, resistive MHD code. The code incorporates the methods of local iterations and flux-corrected-transport. The code is described in our earlier investigation of Bondi accretion to a non-rotating magnetized star (Toropin et al. 1999), (Toropina et al. 2003). The equations for resistive MHD are

$$\frac{\partial \rho}{\partial t} + \nabla \cdot (\rho \mathbf{v}) = 0, \quad (1)$$

$$\rho \frac{\partial \mathbf{v}}{\partial t} + \rho (\mathbf{v} \cdot \nabla) \mathbf{v} = -\nabla p + \frac{1}{c} \mathbf{J} \times \mathbf{B} + \mathbf{F}^g, \quad (2)$$

$$\frac{\partial \mathbf{B}}{\partial t} = \nabla \times (\mathbf{v} \times \mathbf{B}) + \frac{c^2}{4\pi\sigma} \nabla^2 \mathbf{B}, \quad (3)$$

$$\frac{\partial (\rho \varepsilon)}{\partial t} + \nabla \cdot (\rho \varepsilon \mathbf{v}) = -p \nabla \cdot \mathbf{v} + \frac{\mathbf{J}^2}{\sigma}. \quad (4)$$

We assume axisymmetry ($\partial/\partial\phi = 0$), but calculate all three components of \mathbf{v} and \mathbf{B} . The equation of state is taken to be that for an ideal gas, $p = (\gamma - 1)\rho\varepsilon$, with specific heat ratio $\gamma = 7/5$. The equations incorporate Ohm's law $\mathbf{J} = \sigma(\mathbf{E} + \mathbf{v} \times \mathbf{B}/c)$, where σ is the electrical conductivity. The associated magnetic diffusivity, $\eta_m \equiv c^2/(4\pi\sigma)$, is considered to be a constant within the computational region. In equation (2) the gravitational force, $\mathbf{F}^g = -GM\rho\mathbf{R}/R^3$, is due to the central star.

We use a cylindrical, inertial coordinate system (r, ϕ, z) with the z -axis parallel to the star's dipole moment μ and rotation axis $\boldsymbol{\Omega}$.

The equatorial plane is treated as symmetry plane. The vector potential \mathbf{A} is calculated so that $\nabla \cdot \mathbf{B} = 0$ at all times. The star rotates with angular velocity $\boldsymbol{\Omega}_* = \Omega_* \hat{\mathbf{z}}$. The intrinsic magnetic field of the star is taken to be an aligned dipole, $\mathbf{B} = [3\mathbf{R}(\boldsymbol{\mu} \cdot \mathbf{R}) - R^2\boldsymbol{\mu}]/R^5$ with $\boldsymbol{\mu} = \mu \hat{\mathbf{z}}$ and vector-potential $\mathbf{A} = \boldsymbol{\mu} \times \mathbf{R}/R^3$.

We measure length in units of the Bondi radius $R_B \equiv GM/c_\infty^2$, with c_∞ the sound speed at infinity, density in units of the density at infinity ρ_∞ , and magnetic field strength in units of B_0 which is the field at the pole of the numerical star ($r = 0, z = Z_s$). Pressure is measured in units of $B_0^2/8\pi$. The magnetic moment is measured in units of $\mu_0 = B_0 R_B^3/2$.

Simulations were done in a cylindrical region ($0 \leq z \leq Z_{max}$, $0 \leq r \leq R_{max}$). The size of the region is less than the sonic radius of the Bondi flow R_s : $R_{max} = Z_{max} = R_s/\sqrt{2}$. Thus matter inflows supersonically to the computational region. The inflow rate is taken to be the Bondi accretion rate, $\dot{M}_B = 4\pi\lambda(GM_*)^2\rho_\infty/c_\infty^3$, where $\lambda = 0.625$ for $\gamma = 7/5$. A uniform (r, z) grid with 513×513 cells was used.

Initially, the density $\rho(r, z)$ and the velocity $\mathbf{v}(r, z)$ are taken to be the values given by the Bondi (Bondi 1952) solution. Thus, initially $v_\phi = 0$. Also, initially the vector potential \mathbf{A} was taken to that of a dipole so that $B_\phi = 0$. The star was initialized to be rotating at the rate Ω_* .

At the outer boundaries, $r = R_{max}$ and $z = Z_{max}$, the variables $(\rho, v_r, v_z, \varepsilon)$ are fixed and equal to the values for the Bondi flow which has $v_\phi = 0$. The inflowing matter is unmagnetized with $\mathbf{B} = 0$. At the inner boundary, the vector-potential $\mathbf{A} = \hat{\phi} A_\phi$ of the intrinsic dipole field of the star is determined on the surface of the model star. More detailed description of numerical model you can see in (Romanova et al. 2003).

3. Results

Here, we first discuss simulations for the case $\omega_* = \Omega_*/\Omega_{K*} = 0.5$, $\beta = 10^{-7}$, magnetic diffusivity $\tilde{\eta}_m = 10^{-5}$. For the mentioned values of β and η_m , the magnetospheric radius r_{m0} and corotation radius $r_{cor} = (GM/\Omega_*^2)^{1/3}$ are equal

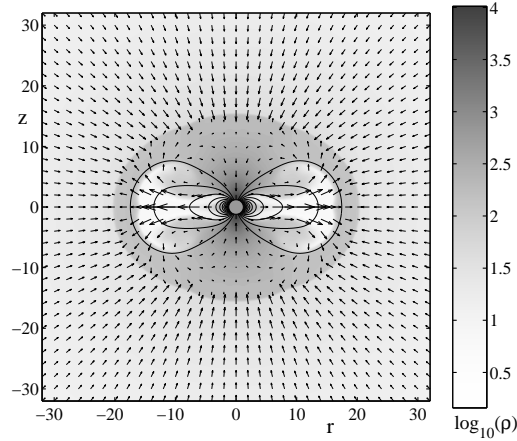


Fig. 1. Matter flow in the “propeller” regime for a star rotating at $\Omega_* = 0.5\Omega_{K*}$ after 6.9 rotation periods of the star. The axes are measured in units of the star’s radius. The background represents the density and the length of the arrows is proportional to the poloidal velocity. The thin solid lines are magnetic field lines.

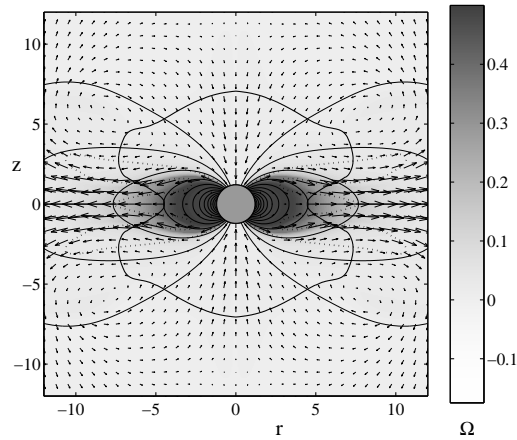


Fig. 2. Enlarged view of Figure 1, the background represents angular velocity $\Omega = v_\phi(r, z)/r$. The bold line represents the Alfvén surface. Dotted line shows sonic surface.

for $\omega_* \approx 0.16$. For smaller angular velocities, $\omega_* < 0.16$, the matter flow around the star is close to that in the non-rotating case. For $\omega_* > 0.16$ the flow exhibits the features expected in the “propeller” regime.

Figure 1 shows the general nature of the flow in the propeller regime. Two distinct regions separated by a shock wave are observed: One is the *external* region where matter inflows with the Bondi rate and the density

and velocity agree well with the Bondi solution. The second is the *internal* region, where the flow is strongly influenced by the stellar magnetic field and rotation. The shock wave, which divides these regions, propagates outward as in the non-rotating case (Toropin et al. 1999), (Toropina et al. 2003). For a rotating star in the propeller regime the shock wave has the shape of an ellipsoid flattened along the rotation axis of the star. The region of the flow

well within the shock wave is approximately time-independent. The accretion rate to the star becomes constant after about 1 – 2 rotation periods of the star.

A new regime of matter flow forms inside the expanding shock wave. The rapidly rotating magnetosphere expels matter outward in the equatorial region. This matter flows radially outward forming a low-density rotating torus. The outflowing matter is decelerated when it reaches the shock wave. There, the flow changes direction and moves towards the rotation axis of the star. However, only a small fraction of this matter accretes to the surface of the star. Most of the matter is expelled again in the equatorial direction by the rotating field of the star. Thus, most of the matter circulates inside this inner region driven by the rapidly rotating magnetosphere.

The solid line in Figure 2 shows the Alfvén surface, where the magnetic energy-density equals the thermal plus kinetic energy-density, $\mathbf{B}^2/8\pi = \varepsilon + \rho v^2/2$. In the equatorial plane, the Alfvén radius is $r_A \approx 4.5R_*$. For $r < r_A$, the magnetic pressure dominates, and the magnetic field is approximately that of a dipole. At larger distances the field is stretched by the outflowing plasma. Matter inside the magnetopause rotates with the angular velocity of the star.

Figure 3 shows the radial dependences of the different radial forces in the equatorial plane. One can see that for $r > 3.5R_*$, the centrifugal force becomes dominant in accelerating the matter outward. However, at larger distances, $r > 5.5R_*$, the pressure gradient force become larger and determines acceleration of matter. Thus, centrifugal and pressure gradient forces accelerate matter in the radial direction. Note, that in most of the region ($r > 4.3R_*$) the magnetic force is negative so that it opposes the matter outflow.

The results we have shown are for a relatively strong propeller. If the rotation rate is smaller, the matter outflow become less intense. For $\Omega_* < 0.16$, no equatorial outflow is observed and the shock wave becomes more nearly spherical as it is in the non-rotating case. On the other hand the shock wave becomes more a more flattened ellipsoid for larger Ω_* .

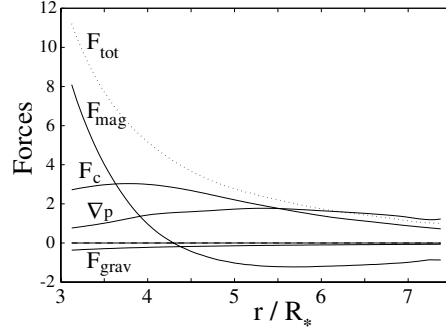


Fig. 3. The radial dependence of the different radial forces acting in the equatorial plane; $F_{\text{mag}} = (\mathbf{J} \times \mathbf{B})_r/c$ is the magnetic force (per unit volume), $F_c = \rho v_\phi^2/r$ is the centrifugal force, $\nabla p = (\nabla p)_r$ is minus the pressure gradient force, $F_{\text{grav}} = -\rho(\nabla\Phi_{\text{grav}})_r$ is the gravitational force, and F_{tot} is the total radial force.

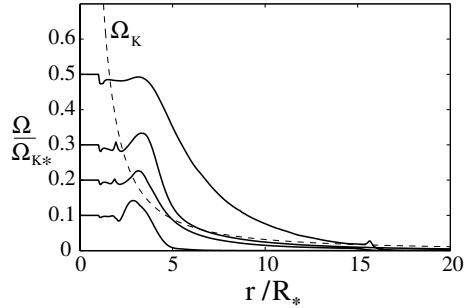


Fig. 4. Angular velocity of matter $\Omega = v_\phi/r$ versus r in the equatorial region for different angular velocities of the star. The dashed line represents the Keplerian angular velocity $\Omega_K = \sqrt{GM/r^3}$.

Matter rotates rigidly inside the Alfvén radius r_A while at large distances $\Omega = v_\phi/r$ decreases, see Figure 4.

Figure 5a shows that the accretion rate to the star decreases as the angular velocity of the star increases, $\dot{M}/\dot{M}_B \propto \omega_*^{-1.0}$. Figure 5b shows that the accretion rate to the star decreases as the star's magnetic moment increases, $\dot{M}/\dot{M}_B \propto \mu^{-2.1}$. We have also done a number of simulation runs for different magnetic diffusivities in the range $\tilde{\eta}_m =$

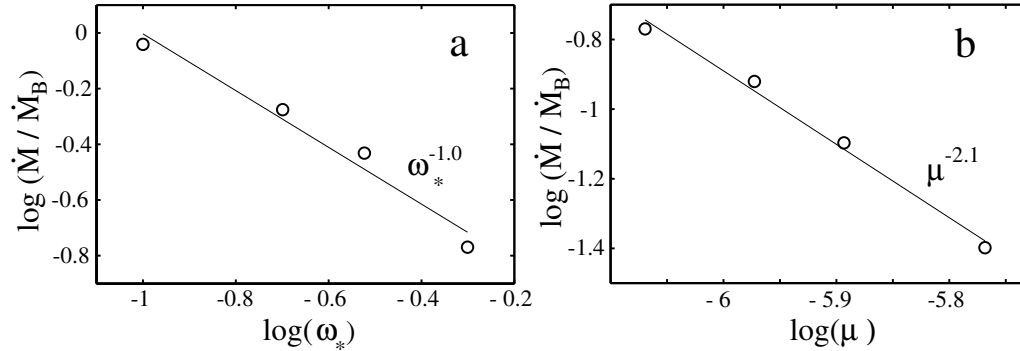


Fig. 5. The left-hand panel (a) shows the fraction of Bondi accretion rate reaching the star as a function of the star's angular velocity $\omega_* = \Omega_*/\Omega_{K*}$. The right-hand panel (b) shows the dependence on the magnetic moment μ for $\Omega_* = 0.5\Omega_K$.

$10^{-6} - 10^{-4.5}$, and from this we conclude that $\dot{M}/\dot{M}_B \propto (\eta_m)^{0.7}$.

4. Conclusions

Axisymmetric magnetohydrodynamic simulations of Bondi accretion to a rotating magnetized star in the propeller regime of accretion have shown that:

(1) A new regime of matter flow forms around a rotating star. Matter falls down along the axis, but only a small fraction of the incoming matter accretes to the surface of the star. Most of the matter is expelled radially in the equatorial plane by the rotating magnetosphere of the star. A low-density torus forms in the equatorial region which rotates with velocity significantly larger than the radial velocity. Large scale vortices form above and below the equatorial plane.

(2) The accretion rate to the star is much less than the Bondi accretion rate and decreases as (a) the star's rotation rate increases ($\propto \Omega_*^{-1.0}$), (b) as the star's magnetic moment increases ($\propto \mu^{-2.1}$), and as the magnetic diffusivity decreases [$\propto (\eta_m)^{0.7}$].

(3) Because the accretion rate to the star is less than the Bondi rate, a shock wave forms in our simulations and propagates outward. It has the shape of an ellipsoid flattened along the rotation axis of the star.

Acknowledgements. This work was supported by NSF grant AST 0307817, by RFBR grant 05-02-17697 and Programme "Nonstationary astronomical events". We thank Dr. V.V. Savelyev for the development of the original version of the MHD code used in this work.

References

- Bondi, H. 1952, MNRAS, 112, 195
- Davidson, K., & Ostriker, J.P. 1973, ApJ, 179, 585
- Goldreich, P., & Julian, W.H. 1969, ApJ, 157, 869
- Illarionov, A.F., & Sunyaev, R.A. 1975. A&A, 39, 185
- Lipunov, V.M. 1992, *Astrophysics of Neutron Stars*, (Berlin: Springer Verlag)
- Romanova, M.M., Toropina, O.D., Toropin, Yu.M., & Lovelace, R.V.E. 2003, ApJ, 588: 400-407
- Shapiro, S.L., & Teukolsky, S.A. 1983, "Black Holes, White Dwarfs, and Neutron Stars", (Wiley-Interscience)
- Shvartsman, V.F. 1970, Radiofizika, 13, 1852
- Toropin, Yu.M., Toropina, O.D., Savelyev, V.V., Romanova, M.M., Chechetkin, V.M., & Lovelace, R.V.E. 1999, ApJ, 517, 906
- Toropina, O.D., Romanova, M.M., Toropin, Yu.M., & Lovelace, R.V.E. 2003, ApJ, 593: 472-480